

# FocalUNETR: A Focal Transformer for Boundary-aware Segmentation of CT Images

Chengyin Li<sup>1</sup>, Hassan Bagher-Ebadian<sup>2</sup>, Vikram Goddla<sup>3</sup>, Indrin J. Chetty<sup>2</sup>,  
and Dongxiao Zhu<sup>1</sup>

<sup>1</sup> Wayne State University, Department of Computer Science, Detroit, MI, USA

<sup>2</sup> Henry Ford Cancer Institute, Department of Radiation Oncology, Detroit, MI, USA

<sup>3</sup> Detroit Country Day School, Beverly Hills, MI, USA  
dzhu@wayne.edu

**Abstract.** Computed Tomography (CT) based precise prostate segmentation for treatment planning is challenging due to (1) the unclear boundary of prostate derived from CT’s poor soft tissue contrast, and (2) the limitation of convolutional neural network based models in capturing long-range global context. Here we propose a focal transformer based image segmentation architecture to effectively and efficiently extract local visual features and global context from CT images. Furthermore, we design a main segmentation task and an auxiliary boundary-induced label regression task as regularization to simultaneously optimize segmentation results and mitigate the unclear boundary effect, particularly in unseen data set. Extensive experiments on a large data set of 400 prostate CT scans demonstrate the superior performance of our focal transformer to the competing methods on the prostate segmentation task.

**Keywords:** Focal Transformer · Image Segmentation · Multi-Task Learning · Computed Tomography.

## 1 Introduction

Prostate cancer is responsible for one of the leading cancer-caused deaths in adult males [25]. External beam radiation therapy (EBRT) is a most commonly used treatments for prostate cancer [7] where precise prostate segmentation of CT images is a crucial step in the EBRT planning to maximize the delivery of radiation doses to tumor tissues while minimizing harm to the surrounding healthy tissues.

While manual delineation is time and labor consuming and frequently plagued by significant inter-operator variation, several automated segmentation methods have been proposed to alleviate the clinician’s burden. Fully convolutional networks (FCN), such as U-Net [26] and its variants [23,2,15,18] have been successfully applied to medical image segmentation tasks. However, the limitation of convolution operation in capturing the long-range relation across global context information still exists [6,19,13], resulting in a subpar performance. On the other hand, accurate prostate segmentation of CT images remains challenging due to

the unclear prostate boundary caused by the low contrast of CT images and the large variance of shapes and sizes across different individuals [30,14].

Considering U-Net, one of the most widely used techniques, uses an FCN-based encoder-decoder setup with skip connections to preserve details in extracting the local visual features. Yet, incorporating a self-attention mechanism to enhance the FCN-based encoder’s ability of capturing the global context is desirable [1]. Transformer-based encoders leveraging the self-attention mechanism show great promise in this regard. Transformers was initially designed to capture long-term dependencies of sequential data with stacked self-attention layers [29] and achieved great success in National Language Processing (NLP) tasks. Inspired by this, Dosovitskiy et al. [8] proposed the Vision Transformer (ViT) by formulating image classification as a sequence prediction task of the image patch (region) sequence, thereby capturing long-term dependencies within the input image. TransUNet [6] successfully adapts the ViT to the medical image segmentation task, where the encoder consists of the FCN-based layers followed by several layers of transformer (multi-head self-attention module) to better capture the global context from medical image inputs. The subsequent studies [28,33,4,16] follow a similar route. However, learning the long-term dependencies that typically contain precise spatial information in low-level feature maps requires more than a few transformer layers for high-level feature inputs.

More recently, Swin Transformer [21] demonstrated that it can simultaneously learn long-range global context and extract hierarchical feature maps from natural images. Based on this idea, SwinUNet [3] utilizes hierarchical Swin Transformer blocks to construct both encoder and decoder with a U-Net-like architecture. DS-TransUNet [19] adds on the more parallel encoder to process the input with a different resolution. SwinUNETR [27] uses a pre-training on a large medical image data set. Despite their usefulness, these fine-grain ViT-based approaches use standard self-attention to capture short- and long-range interactions. As such, they suffer from high computational costs and an explosion of time and memory costs, especially when the feature map size becomes large. The focal transformer [32] employs a focal self-attention mechanism via both fine-grained local and coarse-grained global interactions. Therefore, it can efficiently and effectively capture both short- and long-range visual feature dependencies to improve the performance of objection detection task on the benchmark natural image data sets. To the best of our knowledge, it has not been generalized for extracting visual features to tackle medical image segmentation task. Particularly, to mitigate the unclear organ boundary and the large variance of shapes and sizes in prostate CT scans, we apply a Gaussian kernel over the boundary of ground truth contour [20] via an auxiliary boundary-aware regression task (Figure 2B). This auxiliary task serves as a regularization term for the main mask generation task (Figure 2A), further improving the generalizability of our model to the unseen test sets.

Here we propose a FocalUNETR (Focal UNet Transformers), a novel focal transformer architecture for CT-based image segmentation accounting for the

unclear boundary of CT contours and we summarize our main contributions as follows:

- We propose FocalUNETR, a new focal transformer model for CT-based prostate segmentation utilizing *focal self-attention* to hierarchically learn the feature maps accounting for both short- and long-range visual dependencies efficiently and effectively.
- We tackle the CT-specific unclear boundary challenge by designing an auxiliary task of kernel regression as regularization to the main task of segmentation mask generation.
- We evaluate our proposed method on a large 400-patient CT image dataset, demonstrating an improved performance of prostate segmentation over with state-of-the-art methods.

## 2 Related Work

### 2.1 Prostate Segmentation

Existing prostate segmentation methods can be broadly classified into three types: multi-atlas-based methods, deformable model-based methods, and learning-based methods. In this section, we will review the most related learning-based methods, particularly the state-of-the-art deep learning methods.

In general, conventional learning-based approaches for building models have two major components: (a) extraction of hand-crafted features to represent target organs, and (b) classification/ regression model for segmentation. For instance, Glocker et al. [11] developed a supervised forest model that uses both class and structural information to jointly perform pixel classification and shape regression. To enhance the segmentation performance, Chen and Zheng [5] selected the most important features from the complete feature set using a hierarchical landmark detection method. Gao et al. [9] utilized multi-task random forests to perform the segmentation of prostate, bladder, rectum, left and right femoral heads tasks, jointly with a displacement regression task. Since these methods are typically created using low-dimensional hand-crafted features, their performance may be constrained, particularly when the inputs have a unclear boundary, as in the case of CT-based prostate images.

In contrast to the conventional learning techniques, deep learning methods can automatically extract multi-level feature representations from the input images. For example, a 2D U-Net model was utilized to learn a mapping function that converts each slice CT image to the corresponding segmented mask for prostate, bladder, and rectum in male pelvic [17]. Balagopal et al. [2] proposed an automated workflow for male pelvic CT image segmentation by utilizing a 2D volume localization network followed by a 3D segmentation network for volumetric segmentation of prostate, bladder, rectum, and femoral heads. Both are based on U-Net with an encoder-decoder architecture. To better address the unclear prostate boundary in CT images, He et al. [14] proposed a multi-task learning strategy that combined the main prostate segmentation task with

an auxiliary prostate boundary delineation task. Wang et al. [30] developed a boundary coding representation via a dilation and erosion process over the original segmentation mask. These two studies also adopted the U-Net architecture for segmentation. Despite its success, these FCN models usually fail to capture the long-range global context information due to the induced bias for convolutional operations. As a result, subpar performance may occur, especially when large variation in shapes and sizes from different individuals exists for the prostate segmentation task.

## 2.2 ViT-based Medical Image Segmentation

Motivated by Transformer’s capacity to capture the long-range global relations, Dosovitskiy et al. [8] proposed the ViT by formulating image classification as a sequence prediction task of the image patch sequence, thereby capturing long-term dependencies within the input image. TransUNet [6] is among the first to successfully use ViT for medical image segmentation via using pre-trained weights from image classification. Both convolutional layers serve as the main body for feature extraction, and transformers are used to capture the long-range global context. Some subsequent studies [28,33,4] followed a similar route; however, several layers of transformers are not adequate to learn the long-term dependencies with precise spatial information in the hierarchical feature maps.

To address the above issue, researchers have introduced self-attention into convolution operation [31,34,10] to perform medical image segmentation. For example, Gao et al. [10] integrated self-attention into a CNN for enhancing medical image segmentation. Zhou et al. [34] proposed a hybrid model with interleaved convolution and self-attention in both encoder and decoder modules. Although these methods achieve improved performance, they need carefully design the convolution and self-attention modules, limiting the scalability of developing more advanced transformer architectures. Recently, Swin Transformer [21] demonstrated a linear complexity in self-attention calculation for long-range context learning and generating hierarchical feature maps simultaneously. Based on this idea, SwinUNet [3] utilized hierarchical transformer blocks to construct the encoder and decoder within a U-Net-like architecture and DS-TransUNet [19] added on the more parallel encoder to process the input with a different resolution, and SwinUNETR [27] used pre-training with a large medical image data set. Nonetheless, they focus too much on learning the global long-range dependencies only with fine-grained global interactions without exploring how to efficiently long-range visual dependencies for dense medical image segmentation prediction tasks.

## 3 Methods

### 3.1 FocalUNETR

Our FocalUNETR architecture shares a similar multi-scale design in [12,27], which allows us to obtain hierarchical feature maps at different stages. As shown

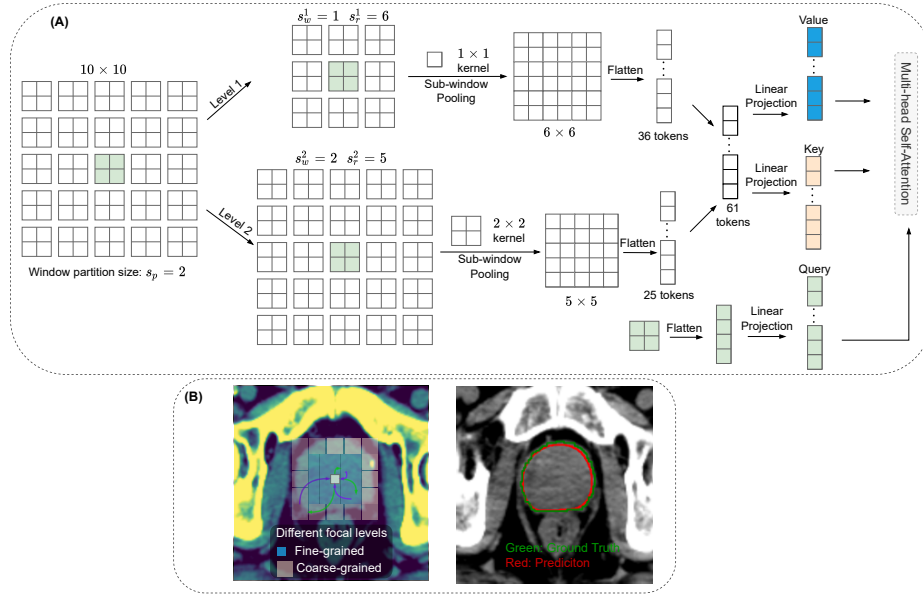


Fig. 1: An illustration of focal self-attention mechanism for medical image segmentation. (A) The focal self-attention mechanism, and (B) An example of perfect boundary matching using focal self-attention for prostate CT image segmentation task.

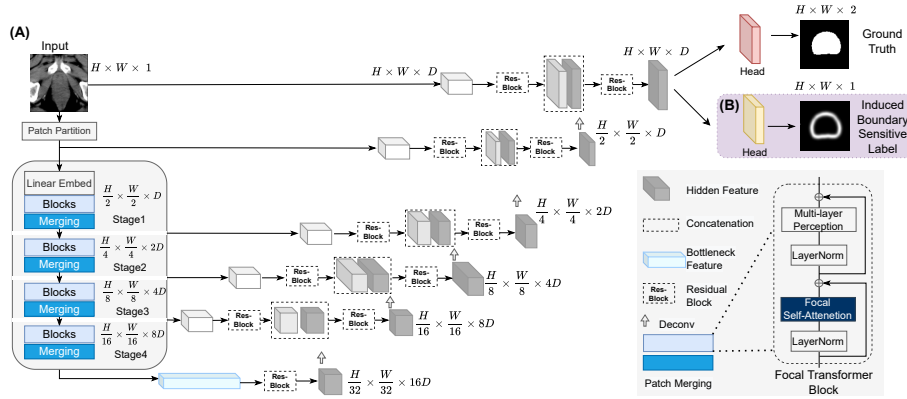


Fig. 2: (A) The architecture of FocalUNETR as the main task for segmentation mask generation, and (B) The auxiliary task designed for mitigating the unclear boundary issue in CT images.

in Figure 2A, a medical image input to the encoder is  $\mathcal{X} \in \mathcal{R}^{C \times H \times W}$ , where  $H, W$  are the spatial height, width and  $C$  is the number of channels. We firstly use a patch with resolution of  $(H', W')$  to split the input into a sequence of tokens with dimension of  $\lceil \frac{H}{H'} \rceil \times \lceil \frac{W}{W'} \rceil$  and project them into an embedding space with dimension  $D$ . The self-attention is computed at two focal levels as shown in Figure 1, fine-grain and coarse-grain. Instead of using all tokens at the fine-grain level, we propose to attend to the fine-grain tokens only locally, but to the coarse-grained (summarized) ones globally. Therefore, it can cover as many regions as standard self-attention to enable long-range self-attention yet with much lower computational cost due to a much smaller number of surrounding (summarized) tokens. In practice, we perform focal self-attention at the window level to efficiently extract the surrounding tokens for each query position. Given a feature map of  $x \in \mathcal{R}^{d \times H'' \times W''}$  with spatial size  $H'' \times W''$  and  $d$  channels, we first partition it into a grid of windows with size  $s_w \times s_w$ . Then, we find the surroundings for each window rather than individual tokens. In the following, we elaborate on the window-wise focal self-attention.

For window-wise focal self-attention [32] (Figure 1A), there are three terms  $\{L, s_w, s_r\}$ . Focal levels  $L$  is the number of granularity levels we extract the tokens for our focal self-attention. We demonstrate two examples of focal levels (fine and coarse). We show two focal levels, (fine and coarse in Figure 1B). Focal window size  $s_w^l$  is the size of sub-window on which we get the summarized tokens at level  $l \in \{1, \dots, L\}$ . Focal region size  $s_r^l$  is the number of sub-windows horizontally and vertically in attended regions at level  $l$ . The focal self-attention module proceeds in two main steps, sub-window pooling, and attention computation. In sub-window pooling step, an input feature map  $x \in \mathcal{R}^{d \times H'' \times W''}$  is split into a grid of sub-windows with size  $\{s_w^l, s_r^l\}$  followed by a simple linear layer  $f_p^l$  to pool the sub-windows spatially. The pooled feature maps at different levels  $l$  provide rich information at both fine-grain and coarse-grain, where  $x^l = f_p^l(\hat{x}) \in \mathcal{R}^{d \times \frac{H''}{s_r^l} \times \frac{W''}{s_r^l}}$ , and  $\hat{x} = \text{Reshape}(x) \in \mathcal{R}^{(d \times \frac{H''}{s_w^l} \times \frac{W''}{s_w^l}) \times (s_w^l \times s_r^l)}$ . After obtaining the pooled feature maps  $x^l$ , we calculate the query at the first level and key and value for all levels using three linear projection layers  $f_q, f_k$  and  $f_v$ :

$$Q = f_q(x^1), K = \{K^l\}_1^L = f_k(\{x^1, \dots, x^L\}), V = \{V^l\}_1^L = f_v(\{x^1, \dots, x^L\}).$$

For the queries inside the  $i$ -th window  $Q_i \in \mathcal{R}^{d \times s_w \times s_w}$ , we extract the  $s_r^l \times s_r^l$  keys and values from  $K^l$  and  $V^l$  around the window where the query lies in and then gather the keys and values from all  $L$  to obtain  $K_i = \{K_1, \dots, K_L\} \in \mathcal{R}^{s \times d}$  and  $V_i = \{V_1, \dots, V_L\} \in \mathcal{R}^{s \times d}$ , where  $s = \sum_{l=1}^L (s_r^l)^2$ . Finally, a relative position bias is added to compute the focal self-attention for  $Q_i$  by

$$\text{Attention}(Q_i, K_i, V_i) = \text{Softmax}\left(\frac{Q_i K_i^T}{\sqrt{d}} + B\right) V_i,$$

where  $B = \{B^l\}_1^L$  is the learnable relative position bias [32].

The encoder uses a patch size of  $2 \times 2$  with a feature dimension of  $2 \times 2 \times 1 = 4$  (*i.e.* single input channel CT) and a  $D$ -dimensional embedding space (*e.g.*,

64). Moreover, the overall architecture of the encoder consists of four stages of focal transformer blocks. Between every stage, a patch merging layer is used to reduce the resolution by a factor of 2. The hierarchical representations of the encoder at different stages are used in downstream applications such as CT-based prostate segmentation for multi-scale feature extraction.

By using skip connections, the FocalUNETR encoder (Figure 2A) connects to a CNN-based decoder at each resolution to build a “U-shaped” network for downstream applications such as segmentation. Following this, we concatenate the encoder output with the processed input volume features and feed them into a residual block for the prostate segmentation task, followed by a final  $1 \times 1$  convolutional layer with a proper activation function (i.e., softmax), the required number of class-based probabilities is obtained.

### 3.2 Multi-Task Learning

For the main task of mask prediction (Figure 2), we use a combination of Dice loss and Cross-Entropy loss to evaluate the pixel-wise agreement between the prediction and the ground truth. The objective function for the main segmentation head is:

$$L_{seg} = L_{dice}(\hat{p}_i, G) + L_{ce}(\hat{p}_i, G),$$

where  $\hat{p}_i$  and  $G$  respectively denote the prediction probabilities from the main task and ground truth mask given an input image  $i$ .  $\hat{p}_i$  is given by the main-task,  $\hat{p}_i = \text{FocalUNETR}(\mathcal{X}, w)$ , where  $w$  is the weights of our model.

To better capture the unclear boundary for the CT-based medical segmentation task, we design an auxiliary task to predict a boundary-aware label besides the main head for generating a segmented mask. We attach convolution layers to the decoder as the reconstruction head (Figure 2B). The boundary-aware labels are generated considering the pixels near the contour as sub-ground truths. Inspired by [22,14], we formulate each contour point and its surrounding pixels into a Gaussian distribution, with a kernel of  $\sigma$  (i.e.,  $\sigma = 1.6$  here). Then a soft label heatmap in the form of a *Heatsum* function [14] can be generated, and we utilize it as a regression task trained by minimising mean-squared error instead of treating it as a single pixel boundary segmentation problem. Given the ground truth of contour  $G_i^C$  induced from the segmentation mask for an input image  $i$ , the reconstructed out probability is denoted as  $\hat{p}_i^C$ . A regression loss is used for this task:

$$L_{reg} = \frac{1}{N} \sum_i \|\hat{p}_i^C - G_i^C\|_2,$$

where  $N$  is the total number of images. This auxiliary task can be trained simultaneously with the main segmentation task.

Multi-task learning is formulated as a main task regularized by auxiliary tasks. The overall loss function is a combination of  $L_{seg}$  and  $L_{reg}$ :

$$L = \lambda_1 L_{seg} + \lambda_2 L_{reg},$$

where  $\lambda_1$  and  $\lambda_2$  are two hyper-parameters of weighting the mask prediction loss and contour regression loss. After tuning hyper-parameters with grid-search, we find the optimal setting of  $\lambda_1 = \lambda_2 = 0.5$ .

## 4 Experiments

### 4.1 Methods for Comparison

We compare the performance of FocalUNETR with multiple state-of-the-art segmentation models. For FCN-based models: UNet [26] builds on top of the fully convolutional networks with a U-shaped architecture to capture context information. The ResUNet is similar to UNet in architecture, but it uses residual blocks as the building block. UNet++ [35] is a variant of UNet. It introduces nested, dense skip connections in the encoder and decoder sub-networks, which can reduce the semantic gap between the feature maps of encoder and decoder sub-networks for better feature fusion. Attention UNet [24] introduces an attention gating module to UNet. The attention gate model learns to suppress irrelevant regions in an input image while highlighting salient features useful for a specific task. Here we implement all models for 2D setting, due to the large space distance variance between different CT cases.

For Transformer-based models: TransUNet [6] is an early attempt of Transformers on medical image segmentation. It uses a R50-ViT as the encoder and employs a UNet decoder for 2D medical image segmentation. Specifically, the images is first fed to the ResNet50 backbone to obtain the feature map ( $16\times$  down-sampled), and then processed by ViT for further modeling. SwinUNet [3] is a pure Transformer model for 2D medical image segmentation, which uses SwinTransformer blocks in a UNet-like encoder decoder structure. It first divides images into  $4\times 4$  patches and then projects patches into token embeddings. The tokens are processed by interleaved window-based attention and shifted window-based attention module. The window-based attention compute the attention locally and propagate information across windows by shifting the window.

### 4.2 Experiment Setup

We systematically evaluate the performance of FocalUNETR on a large in-house CT data set with 400 cases for prostate gland segmentation. For this dataset, we randomly split it into 280, 40, and 80 cases for training, validation, and test sets. In data pre-processing, we resample all images to a spatial resolution of  $1.0\times 1.0\times 1.5\text{ mm}^2$ . A  $128\times 128\times 64$  voxel patch at the center of each image was cropped for training. A pixel-wise linear transformation was applied to assign HU values to intensity levels between 0 and 1. We train all models but TransUNet (with ViT pretrained on ImageNet) from scratch for 100 epochs with a default batch size of 24, and use the exponentially learning rate scheduler with a base learning rate of 0.01. We use the SGD (stochastic gradient descent) optimizer with a batch size of 32 on a NVIDIA A100 GPU, momentum and weight decay



are set to 0.9 and 1e-4 respectively. Data augmentation is applied on the fly during model training to alleviate overfitting, including random rotation and flip. All images are resampled with bi-linear interpolation to  $224 \times 224$  before entering the models.

### 4.3 Evaluation Metrics

We use Dice score and 95% Hausdorff Distance (HD) to evaluate the accuracy of segmentation in our experiments. The Dice similarity coefficient (DSC) evaluates the overlap of the predicted and ground truth segmentation map:

$$DSC = \frac{2|P \cap G|}{|P| + |G|},$$

where  $P$  indicates the predicted segmentation map and  $G$  denotes the ground truth. A DSC of 1 indicates a perfect segmentation while 0 indicates no overlap at all. Hausdorff distance (HD) measures the largest symmetrical distance between two segmentation maps:

$$d_H(P, G) = \max\{\sup_{p \in P} \inf_{g \in G} d(p, g), \sup_{g \in G} \inf_{p \in P} d(p, g)\},$$

where  $d(\cdot)$  represents the Euclidean distance, sup and inf denote supremum and infimum, respectively. We employ 95% HD to eliminate the impact of a very small subset of the outliers.

Table 1: Quantitative performance comparison on the in-house prostate CT datasets in terms of average Dice similarity coefficient, and average 95% Hausdorff distance.

Methods	Avg DSC (%)	Avg 95HD (mm)
UNet	$84.21 \pm 1.21$	$6.73 \pm 0.89$
ResUNet	$84.82 \pm 1.33$	$6.89 \pm 1.36$
UNet++	$85.54 \pm 1.62$	$6.53 \pm 1.12$
Attn UNet	$85.62 \pm 0.98$	$6.58 \pm 0.98$
TransUNet	$85.12 \pm 2.32$	$6.35 \pm 1.32$
SwinUNet	$86.31 \pm 1.72$	$6.10 \pm 1.28$
FocalUNETR (ours)	<b><math>87.67 \pm 1.42</math></b>	<b><math>5.62 \pm 1.17</math></b>
FocalUNETR + Multi-Task	<b><math>88.15 \pm 1.39</math></b>	<b><math>5.53 \pm 1.01</math></b>

### 4.4 Experimental Results

All methods are evaluated using two metrics, i.e., Dice and 95% Hausdorff Distance (95HD[mm]). Table 1 tabulates the segmentation results on the 400

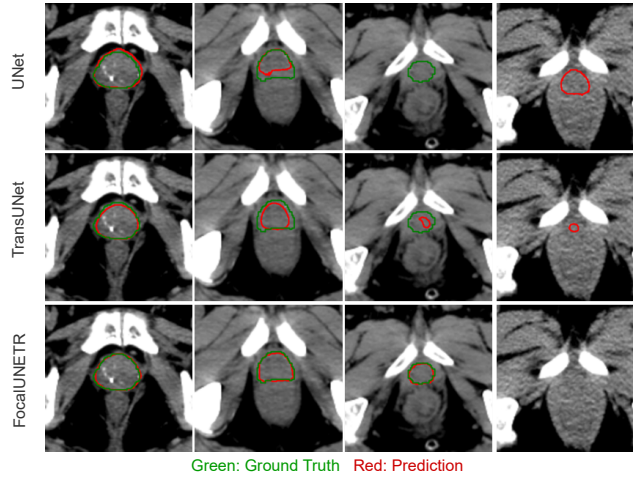


Fig. 3: Qualitative results of prostate segmentation by comparing our FocalUNETR with two other representative segmentation models. For fair comparison, all methods are trained with only main segmentation task.

CT cases data set. We compare the FocalUNETR with both the FCN-based and transformer-based models. Both metrics identify the superior of our FocalUNETR model compared with others. Specifically, the UNet and its variants demonstrate a relatively low performance due to their limited capability of capturing long-range global context. TransUNet and SwinUNet built with ViT and Swin transformers achieve better performance than the UNets. However, these two models still suffer from effectively learning the local information and global context simultaneously and show subpar performance than our focal transformer based FocalUNETR. Furthermore, using the multi-task training strategy, our FocalUNETR model demonstrates better performance on the CT images with unclear boundary.

Figure 3 shows the qualitative results for prostate segmentation. We compared our FocalUNETR with two other representative models, UNet and TransUNet. All methods perform well for easy cases, but our FocalUNETR can be even better. For more challenging cases (irregular shape, unclear boundary, small size), FocalUNETR performs much better than others. FocalUNETR is less likely to give the false prediction (false positives) for CT images without a foreground mask.

#### 4.5 Ablation Study

During the training of FocalUNETR, we find that the embedding space dimension ( $D$ ) has a relatively significant impact on the final segmentation accuracy. By increasing the  $D$  from 48 to 64 (introducing more parameters), the segmentation performance improves accordingly on both DSC and 95HD metrics (Table

2). We do not explore more complex settings of FocalUNETR due to limited computing resources.

Table 2: The effect of embedding space dimension on segmentation performance.

$D$	Avg DSC (%)	Avg 95HD (mm)	Param (M)
48	$86.53 \pm 1.65$	$5.95 \pm 1.29$	25.5
64	<b><math>87.67 \pm 1.42</math></b>	<b><math>5.62 \pm 1.17</math></b>	57.8

## 5 Conclusion

To better capture the local visual features and global contexts in medical images, we present a novel focal transformer based segmentation architecture, FocalUNETR. The learned hierarchical features are effective in extracting visual features for the main segmentation and auxiliary boundary-aware regression tasks. Furthermore, boundary-aware labels can alleviate the unclear boundary and the large variance in sizes and shapes. Extensive experiments on a large data set with 400 cases of prostate CTs show that our FocalUNETR achieves generally better performance than the state-of-the-art methods on the prostate segmentation task.

## References

1. Alimjan, G., Jiaermuhamaiti, Y., Jumahong, H., Zhu, S., Nurmamat, P.: An image change detection algorithm based on multi-feature self-attention fusion mechanism unet network. *International Journal of Pattern Recognition and Artificial Intelligence* **35**(14), 2159049 (2021)
2. Balagopal, A., Kazemifar, S., Nguyen, D., Lin, M.H., Hannan, R., Owringi, A., Jiang, S.: Fully automated organ segmentation in male pelvic ct images. *Physics in Medicine & Biology* **63**(24), 245015 (2018)
3. Cao, H., Wang, Y., Chen, J., Jiang, D., Zhang, X., Tian, Q., Wang, M.: Swin-unet: Unet-like pure transformer for medical image segmentation. *arXiv preprint arXiv:2105.05537* (2021)
4. Chen, B., Liu, Y., Zhang, Z., Lu, G., Zhang, D.: Transattunet: Multi-level attention-guided u-net with transformer for medical image segmentation. *arXiv preprint arXiv:2107.05274* (2021)
5. Chen, C., Zheng, G.: Fully automatic segmentation of ap pelvis x-rays via random forest regression and hierarchical sparse shape composition. In: *International conference on computer analysis of images and patterns*. pp. 335–343. Springer (2013)
6. Chen, J., Lu, Y., Yu, Q., Luo, X., Adeli, E., Wang, Y., Lu, L., Yuille, A.L., Zhou, Y.: Transunet: Transformers make strong encoders for medical image segmentation. *arXiv preprint arXiv:2102.04306* (2021)

7. D’Amico, A.V., Whittington, R., Malkowicz, S.B., Schultz, D., Blank, K., Broderick, G.A., Tomaszewski, J.E., Renshaw, A.A., Kaplan, I., Beard, C.J., et al.: Biochemical outcome after radical prostatectomy, external beam radiation therapy, or interstitial radiation therapy for clinically localized prostate cancer. *Jama* **280**(11), 969–974 (1998)
8. Dosovitskiy, A., Beyer, L., Kolesnikov, A., Weissenborn, D., Zhai, X., Unterthiner, T., Dehghani, M., Minderer, M., Heigold, G., Gelly, S., Uszkoreit, J., Houlsby, N.: An image is worth 16x16 words: Transformers for image recognition at scale. *ICLR abs/2010.11929* (2021)
9. Gao, Y., Shao, Y., Lian, J., Wang, A.Z., Chen, R.C., Shen, D.: Accurate segmentation of ct male pelvic organs via regression-based deformable models and multi-task random forests. *IEEE transactions on medical imaging* **35**(6), 1532–1543 (2016)
10. Gao, Y., Zhou, M., Metaxas, D.N.: Utnet: a hybrid transformer architecture for medical image segmentation. In: *International Conference on Medical Image Computing and Computer-Assisted Intervention*. pp. 61–71. Springer (2021)
11. Glocker, B., Pauly, O., Konukoglu, E., Criminisi, A.: Joint classification-regression forests for spatially structured multi-object segmentation. In: *European conference on computer vision*. pp. 870–881. Springer (2012)
12. Hatamizadeh, A., Tang, Y., Nath, V., Yang, D., Myronenko, A., Landman, B., Roth, H.R., Xu, D.: Unetr: Transformers for 3d medical image segmentation. In: *Proceedings of the IEEE/CVF Winter Conference on Applications of Computer Vision*. pp. 574–584 (2022)
13. He, K., Gan, C., Li, Z., Rekik, I., Yin, Z., Ji, W., Gao, Y., Wang, Q., Zhang, J., Shen, D.: Transformers in medical image analysis: A review. *arXiv preprint arXiv:2202.12165* (2022)
14. He, K., Lian, C., Zhang, B., Zhang, X., Cao, X., Nie, D., Gao, Y., Zhang, J., Shen, D.: Hf-unet: learning hierarchically inter-task relevance in multi-task u-net for accurate prostate segmentation in ct images. *IEEE Transactions on Medical Imaging* **40**(8), 2118–2128 (2021)
15. Isensee, F., Jaeger, P.F., Kohl, S.A., Petersen, J., Maier-Hein, K.H.: nnu-net: a self-configuring method for deep learning-based biomedical image segmentation. *Nature methods* **18**(2), 203–211 (2021)
16. Jiang, J., Elguindi, S., Berry, S.L., Onochie, I., Cervino, L., Deasy, J.O., Veeraraghavan, H.: Nested-block self-attention multiple resolution residual network for multi-organ segmentation from ct. *Medical Physics* (2022)
17. Kazemifar, S., Balagopal, A., Nguyen, D., McGuire, S., Hannan, R., Jiang, S., Owangi, A.: Segmentation of the prostate and organs at risk in male pelvic ct images using deep learning. *Biomedical Physics & Engineering Express* **4**(5), 055003 (2018)
18. Li, X., Bagher-Ebadian, H., Gardner, S., Kim, J., Elshaikh, M., Movsas, B., Zhu, D., Chetty, I.J.: An uncertainty-aware deep learning architecture with outlier mitigation for prostate gland segmentation in radiotherapy treatment planning. *Medical Physics* (2022)
19. Lin, A., Chen, B., Xu, J., Zhang, Z., Lu, G., Zhang, D.: Ds-transunet: Dual swin transformer u-net for medical image segmentation. *IEEE Transactions on Instrumentation and Measurement* (2022)
20. Lin, L., Wang, Z., Wu, J., Huang, Y., Lyu, J., Cheng, P., Wu, J., Tang, X.: Bsdanet: A boundary shape and distance aware joint learning framework for segmenting and classifying octa images. In: *International Conference on Medical Image Computing and Computer-Assisted Intervention*. pp. 65–75. Springer (2021)

21. Liu, Z., Lin, Y., Cao, Y., Hu, H., Wei, Y., Zhang, Z., Lin, S., Guo, B.: Swin transformer: Hierarchical vision transformer using shifted windows. In: Proceedings of the IEEE/CVF International Conference on Computer Vision. pp. 10012–10022 (2021)
22. Ma, J., Wei, Z., Zhang, Y., Wang, Y., Lv, R., Zhu, C., Gaoxiang, C., Liu, J., Peng, C., Wang, L., et al.: How distance transform maps boost segmentation cnns: an empirical study. In: Medical Imaging with Deep Learning. pp. 479–492. PMLR (2020)
23. Milletari, F., Navab, N., Ahmadi, S.A.: V-net: Fully convolutional neural networks for volumetric medical image segmentation. In: 2016 fourth international conference on 3D vision (3DV). pp. 565–571. IEEE (2016)
24. Oktay, O., Schlemper, J., Folgoc, L.L., Lee, M., Heinrich, M., Misawa, K., Mori, K., McDonagh, S., Hammerla, N.Y., Kainz, B., et al.: Attention u-net: Learning where to look for the pancreas. arXiv preprint arXiv:1804.03999 (2018)
25. Parikesit, D., Mochtar, C.A., Umbas, R., Hamid, A.R.A.H.: The impact of obesity towards prostate diseases. *Prostate international* **4**(1), 1–6 (2016)
26. Ronneberger, O., Fischer, P., Brox, T.: U-net: Convolutional networks for biomedical image segmentation. In: International Conference on Medical image computing and computer-assisted intervention. pp. 234–241. Springer (2015)
27. Tang, Y., Yang, D., Li, W., Roth, H.R., Landman, B., Xu, D., Nath, V., Hatamizadeh, A.: Self-supervised pre-training of swin transformers for 3d medical image analysis. In: Proceedings of the IEEE/CVF Conference on Computer Vision and Pattern Recognition. pp. 20730–20740 (2022)
28. Valanarasu, J.M.J., Oza, P., Hacıhaliloglu, I., Patel, V.M.: Medical transformer: Gated axial-attention for medical image segmentation. In: International Conference on Medical Image Computing and Computer-Assisted Intervention. pp. 36–46. Springer (2021)
29. Vaswani, A., Shazeer, N., Parmar, N., Uszkoreit, J., Jones, L., Gomez, A.N., Kaiser, Ł., Polosukhin, I.: Attention is all you need. *Advances in neural information processing systems* **30** (2017)
30. Wang, S., Liu, M., Lian, J., Shen, D.: Boundary coding representation for organ segmentation in prostate cancer radiotherapy. *IEEE transactions on medical imaging* **40**(1), 310–320 (2020)
31. Xie, Y., Zhang, J., Shen, C., Xia, Y.: Cotr: Efficiently bridging cnn and transformer for 3d medical image segmentation. In: International conference on medical image computing and computer-assisted intervention. pp. 171–180. Springer (2021)
32. Yang, J., Li, C., Zhang, P., Dai, X., Xiao, B., Yuan, L., Gao, J.: Focal self-attention for local-global interactions in vision transformers. arXiv preprint arXiv:2107.00641 (2021)
33. Zhang, Y., Liu, H., Hu, Q.: Transfuse: Fusing transformers and cnns for medical image segmentation. In: International Conference on Medical Image Computing and Computer-Assisted Intervention. pp. 14–24. Springer (2021)
34. Zhou, H.Y., Guo, J., Zhang, Y., Yu, L., Wang, L., Yu, Y.: nnformer: Interleaved transformer for volumetric segmentation. arXiv preprint arXiv:2109.03201 (2021)
35. Zhou, Z., Rahman Siddiquee, M.M., Tajbakhsh, N., Liang, J.: Unet++: A nested u-net architecture for medical image segmentation. In: Deep learning in medical image analysis and multimodal learning for clinical decision support, pp. 3–11. Springer (2018)